RESEARCH PAPER

Beta-casein Nanoparticles as an Oral Delivery System for Chemotherapeutic Drugs: Impact of Drug Structure and Properties on Co-assembly

Alina Shapira • Yehuda G. Assaraf • Dikla Epstein • Yoav D. Livney

ABSTRACT

Purpose To develop a novel oral drug delivery system comprising a hydrophobic chemotherapeutic drug entrapped within beta casein (β–CN), a major milk protein, which self-associates into micelles in aqueous solutions. The efficient gastric digestibility of β–CN suggests possible targeting to gastric cancers.

Methods Antitumor drug entrapment was performed by stirring its dimethyl-sulfoxide solution into a phosphate-buffered saline containing β–CN. The association of drugs to β–CN was characterized by spectrophotometry and Trp143 fluorescence quenching; particle-size by dynamic light scattering, and colloidal stability by zeta potential.

Results The optimal drug-to-β–CN molar loading-ratios for paclitaxel and vinblastine at 1 mg/ml β–CN were found to be 7.3 ± 1.2 and 5.3 ± 0.6 and the association constants were $(6.3 \pm 1.0) \cdot 10^3$ M^{-1} and $(2.0 \pm 0.3) \cdot 10^4$ M^{-1}, respectively. Zeta potential analysis suggested that nanoencapsulation by β–CN stabilized all studied drugs in aqueous solution. The initial drug-β–CN association was apparently governed by hydrophobic interactions and at higher drug concentrations, also by electrostatic interactions. Up to the optimal drug:β–CN loading-ratio, ~80% of the particles were below 100 nm in diameter. At higher drug concentrations, particle diameter increased, and bi- or tri-modal particle distributions were observed.

Conclusions Beta–CN forms colloidally-stable nanovehicles of hydrophobic anticancer drugs, and may be used for oral-delivery of chemotherapeutics.

KEY WORDS β-casein micelles · cancer · gastrointestinal tract · hydrophobic chemotherapeutics · targeted oral delivery

A. Shapira · Y. D. Livney
Russell Berrie Nanotechnology Institute
Technion-Israel Institute of Technology
Haifa 32000, Israel

Y. G. Assaraf
The Fred Wyszkowski Cancer Research Laboratory
Faculty of Biology, Technion-Israel Institute of Technology
Haifa 32000, Israel

D. Epstein · Y. D. Livney (✉)
The Laboratory of Biopolymers and Food Nanotechnology
Faculty of Biotechnology & Food Engineering
Technion-Israel Institute of Technology
Haifa 32000, Israel
e-mail: livney@technion.ac.il

ABBREVIATIONS

β–CN	beta casein
c log P	calculated log P values
c pK$_a$	calculated pK$_a$ values
CMC	critical micellization concentration
cryoTEM	cryogenic transmission electron microscopy
DLS	dynamic light scattering
DMSO	dimethyl sulfoxide
F	the fluorescence intensity at a given added ligand (drug) concentration
F_0	the fluorescence intensity at the beginning of the titration
F_1	the fluorescence intensity at the end of the titration
FRET	fluorescence resonance energy transfer
GIT	gastrointestinal tract
IV	intravenous
K_a	the (average) apparent association constant of a single binding site
K_d	the (average) apparent dissociation constant of a single binding site

[L$_F$]	the molar concentration of the free ligand (drug)
log P	log of the octanol-water partition coefficient
n	number of binding sites per protein molecule
PBS	phosphate buffer saline
[P$_F$]	free protein molar concentration
pI	isoelectric pH
pK$_a$	negative log of the association constant (K$_a$)
[PL]	the molar concentration of protein to which ligand is bound
Rg	radius of gyration
Trp	Tryptophan

INTRODUCTION

Many of the current chemotherapeutic drugs for the treatment of multiple human malignancies are administered intravenously (IV). Studies suggest that IV administration of chemotherapeutics is a major source of cost, discomfort and stress to patients, and multiple hospitalizations are required in order to complete the relatively long IV sessions of combination chemotherapeutic regimens (1). The availability of suitable and effective oral therapeutic agents would make a significant contribution to patients' quality of life, may significantly reduce cost and may prove more effective than current treatment modalities.

Beta-casein (β–CN), one of the four main caseins in bovine milk, has a pronounced amphiphilic structure (2,3), which enables it to self-associate under appropriate (i.e. physiological) conditions, thereby forming stable micelle-like structures in aqueous solutions (4,5). Single β–CN molecules have a radius of gyration (Rg) of 4.6 nm and an isoelectric pH (pI) of 5.33 (3). The micelles, containing 15–60 β–CN molecules, have Rg values ranging between 7.3 and 13.5 nm. The critical micellization concentration (CMC) ranges between 0.05 and 0.2% w/v, depending on temperature, pH, solvent composition and ionic strength (6). Previous studies from our laboratory (7) have shown that casein micelles may be utilized as natural nano-delivery vehicles for lipid-soluble vitamins (e.g. vitamin D). In a more recent study (8,9), we have suggested that β–CN nanoparticles may entrap and deliver hydrophobic chemotherapeutics such as mitoxantrone. Few studies have investigated the binding of lipophilic compounds, e.g. vitamin D$_3$ (10), vitamin A (11) and sucrose esters (12), to β–CN. These studies suggested that hydrophobic interactions are largely responsible for the binding of lipid-soluble molecules to β–CN (10).

It has been suggested (13) that β–CN is analogous to a di-block copolymer. As such, β–CN micelles are expected to be extremely more stable than those of low molecular weight surfactant micelles, and the kinetics of release of entrapped hydrophobic molecules are expected to be several orders of magnitude slower compared to release from low molecular weight surfactants (14), which is a major advantage of using β–CN for this task, compared to the use of small surfactants. In this respect, many of the antitumor agents are highly hydrophobic, including *Vinca* alkaloids (e.g. vinblastine and vincristine) (15), epipodophyllotoxins (etoposide and teniposide), taxenes (paclitaxel and docetaxel) (16) and camptothecins (topotecan and irinotecan) (17). The major goal of the current research was to develop a rationally designed drug delivery system comprising hydrophobic anticancer drugs entrapped within β–CN-based nanoparticles. This novel drug delivery system will allow lipid-soluble drugs to be thermodynamically stable in aqueous solutions and thereby readily deliverable to target malignant tumor regions along the gastrointestinal tract (GIT). Since caseins evolved to be easily digestible, the basic nanovehicle is expected to readily release its chemotherapeutic cargo in the stomach. Gastric cancer is a major cause of cancer death worldwide, especially in developing countries (18). Complementary nano-coatings made of other biopolymers will present a programmed degradation pattern and release this antitumor drug cargo at the desired site further down the GIT (e.g. dietary fibers, which are only digested by colon microflora, may be used as external coating for colon targeting). Moreover, as mentioned above, by entrapping drug combinations within these nanoparticles, one may increase the therapeutic index of the chemotherapeutic regimen. The specific aims of the current study were to evaluate the affinity and stoichiometry of association of each of the studied hydrophobic anticancer drugs to β–CN, using absorbance spectra and Trp emission quenching measurements, and to compare the different drugs in terms of the properties of the β–CN-drug nanoparticles formed, characterized by dynamic light scattering, zeta potential, and visual observation. With the aim of gaining some basic conclusions regarding these drug-protein interactions, we chose to study a representative drug from each of several different chemotherapeutic drug families: vinblastine, paclitaxel, docetaxel, and irinotecan, in addition to mitoxantrone, whose entrapment in β–CN we had previously described (8,9). These drugs have different mechanisms of action. Mitoxantrone is a type II topoisomerase inhibitor. It disrupts DNA synthesis and DNA repair; taxanes (Paclitaxel, Docetaxel) bind to β-tubulin, thereby resulting in the promotion of microtubule assembly and the formation of stable, non-functional microtubules, thereby interfering with mitosis, as well as with multiple cellular processes that require intact cytoskeletal structure. Taxanes efficiently induce apoptosis and have anti-angiogenic properties as well; irinoteacan targets topoisomerase I and thus induces single-strand DNA breaks,

thereby blocking cellular DNA replication [17]. Vinblastine also binds to β-tubulin, as do taxanes, but in contradistinction to the latter, vinblastine inhibits tubulin polymerization; by disrupting microtubule polymerization, it blocks mitosis, thereby leading to cell death via apoptosis. These drugs have different chemical properties, as detailed in Table I (log P—log of the octanol-water partition coefficient and pKa values of different functional groups of each drug, which determine the drug's charge at pH 7, were studied here). These properties affect their entrapment capacity within β–CN nanoparticles as well as the nanoparticle characteristics. The chemical structures of the anticancer drugs studied here are depicted in Fig. 1.

MATERIALS AND METHODS

Paclitaxel (T7191, purity >97%), vinblastine sulfate (V1377, purity >97%), and β–CN from bovine milk (C6905, 90% purity) were purchased from Sigma-Aldrich Israel Ltd. (Rehovot, Israel). Irinotecan hydrochloride trihydrate and docetaxel trihydrate were purchased from Iffect Chemphar Co., Ltd. (Shenzehen, China). A 10 mM stock solution of each drug in dimethyl sulfoxide (DMSO) was freshly prepared prior to use. Beta–CN was dissolved at different concentrations in sodium phosphate buffer saline (PBS) pH 7.0, ionic strength 0.1 M. PBS contained 80 mM NaCl, 5.65 mM Na_2HPO_4 and 3.05 mM NaH_2PO_4. The entrapment of each drug in β–CN nanoparticles at different drug:β–CN molar ratios was performed by adding different volumes of the drug solution in DMSO to a β–CN solution in PBS while continuously stirring. The volume percentage of DMSO in PBS did not exceed 6%. The samples were equilibrated ~16 h at room temperature (20–24°C).

Calculation of C log P Values

C log P values were calculated using the ACD/I-Lab Web service (ACD/Log P 8.02) [19].

Calculation of Charge at pH 7

The calculation of pKa values (c pKa) for different ionizing groups was performed using the ACD/I-Lab Web service (ACD/Log P 8.02) [19]. The fraction of charged ionizable groups at each charge at pH 7 was calculated according to Henderson–Hasselbalch equation, e.g.,

$$pH = pKa + \log \frac{[NH_2]}{[NH_3^+]}$$

using the calculated pKa values. This fraction was multiplied by the charge and was summed up to calculate the net charge of the molecule as described in Supplementary Materials.

Spectrophotometric Absorbance Spectra

Absorbance spectra of 1 mg/ml (42 μM) β–CN and of 167 μM vinblastine, irinotecan, paclitaxel, or docetaxel in PBS and 1.67% DMSO (4:1 drug: β–CN molar ratio), against a PBS blank containing 1.67% DMSO, were collected (Fig. 2). Absorbance spectra of 167 μM drug in 1 mg/ml β–CN were collected for each drug, against a PBS blank containing 1.67% DMSO. The spectra were collected using an Ultrospec 3000 spectrophotometer (GE Healthcare, Waukesha, WI, USA).

Tryptophan (Trp) Fluorescence Quenching Measurements

Trp143 is located in the main hydrophobic domain of β–CN. Quenching of protein fluorescence due to energy transfer from this Trp residue to a bound ligand serves to determine the binding affinity [20]. The interaction between paclitaxel-β–CN and vinblastine-β–CN above the CMC of pure β–CN was studied by monitoring the changes in the Trp143 fluorescence emission of β–CN prior to and after the addition of various concentrations of each drug. Trp fluorescence was determined using an excitation of 287 nm, and emission was collected at 332 nm [10], with slit widths of 1 nm on both, using the Fluorolog 3-22 spectrofluorometer (Jobin Yvon; Horiba, Longjumeau, France). Changes in Trp fluorescence were used to evaluate the association of the drugs with β–CN. Assuming the binding sites on the β–CN protein are independent and similar in their binding affinity for the drug [20], the apparent association constant (Ka) of each binding site and the number of binding sites per β–CN molecule (n) were derived from plots of the fluorescence intensity at 332 nm, expressed as the percentage of the fluorescence of the drug-free β–CN vs. drug concentration. Although there is only one reporting site, i.e. Trp143 in the hydrophobic domain of the protein, a higher stoichiometric ratio than 1 can still be obtained if other binding sites of higher or equal affinity exist on the protein and are thus saturated prior to or simultaneously with the reporting site or due to drug aggregate binding to the hydrophobic core of β–CN micellar nanoparticles. The data were analyzed using Matlab (MathWorks), by means of the following equations:

$$F = \frac{F_0[P_F] + F_1[PL]}{[P_F] + [PL]} \tag{1}$$

$$K_d' = \frac{1}{K_a'} = \frac{(n[P_F])[L_F]}{n[PL]} = \frac{[P_F][L_F]}{[PL]} \tag{2}$$

where F is the fluorescence intensity at a given added ligand (drug) concentration, F_0 is the fluorescence intensity at the

Table I Chemical Properties of the Drugs: Vinblastine, Irinotecan, Mitoxantrone, Paclitaxel, Docetaxel

Drug name (Molecular weight, gr/mole)	log P[a]	c log P[b]	pka[c]	c pka[d]	Average charge at pH7[e]
Vinblastine (811.0)	3.4 (15)	4.18	7.4 (28)	16.70; 14.61; 11.32; 7.64; 5.62; 1.23; −3.11	+4.73
Irinotecan (586.7)	4.37 (29)	4.07	8.1 (30)	11.20; 5.45; −1.76; −2.90	+0.03
Mitoxantrone (444.5)	1.099 (31)	3.39	5.99; 8.13 (32)	15.07; 14.47; 9.27; 8.66; 8.61; 7.08; 2.66; −4.18	+1.53
Paclitaxel (853.9)	4.54 (33)	7.38	–[f]	13.63; 13.10; 12.43; 11.90; −2.19	$0\ (-1.25 \cdot 10^{-5})$
Docetaxel (861.9)	3.69 (33)	6.55	–[f]	13.38; 12.9; 12.83; 11.32; 11.20; −1.68	$0\ (-6.31 \cdot 10^{-5})$

[a] log P—log of the octanol-water partition coefficient from literature

[b] c log P—calculated log P values were calculated using the ACD/I-Lab Web service (ACD/Log P 8.02) (17)

[c] pKa values from literature

[d] c pKa—calculated pKa values for different ionizing groups, were calculated using the ACD/I-Lab Web service (ACD/Log P 8.02) (17)

[e] The fraction of charged molecules at each charge at pH 7 was calculated according to Henderson–Hasselbalch equation (e.g. $pH = pKa + \log \frac{[NH]}{[NH_2^+]}$) using the calculated pKa. This fraction was multiplied by the charge and was summed up to calculate the average charge of the molecule as described in Supplementary Materials

[f] not available

beginning of the titration, and F_1 is the fluorescence at the end of the titration (21). For algebraic simplicity, and without reducing generality, it can be assumed that during titration, the ligand molecules occupy all of the binding sites of a protein molecule before starting to occupy sites of the next protein molecule (i.e. a negligible-partial-occupancy assumption). Therefore, if $[P_F]$ is the concentration of free β–CN, and n is the number of binding sites in a protein molecule, then $(n[P_F])$ is the concentration of free (unoccupied) binding sites in the system, $[L_F]$ is the concentration of the free ligand (drug). This assumption also entails that if [PL] is the concentration of protein to which ligand is bound, then n[PL] is the concentration of bound ligand (drug), and K_d' and K_a' are the apparent dissociation and association constants of a single binding site, respectively

(20) (i.e. they represent an equivalent mean affinity of the different sites of the protein). Emission spectrum of pure 1 mg/ml (0.042 mM) β–CN *vs.* spectra of 1 mg/ml β–CN containing paclitaxel and vinblastine solutions at 4:1 drug: β–CN molar ratio were collected at a Trp excitation wavelength of 287 nm using the Fluorolog 3-22 spectrofluorometer.

Nanoparticle Size Distribution and Zeta Potential Analysis

Particle size distribution and zeta potential were determined by a combined dynamic light scattering (DLS) and zeta potential analyzer (NICOMP™ 380, Particle Sizing Systems, Agilent Technologies, Inc., Santa Barbara, CA,

Fig. 1 Chemical structures of the drugs (**A**) vinblastine (**B**) irinotecan (**C**) mitoxantrone (**D**) paclitaxel (**E**) docetaxel.
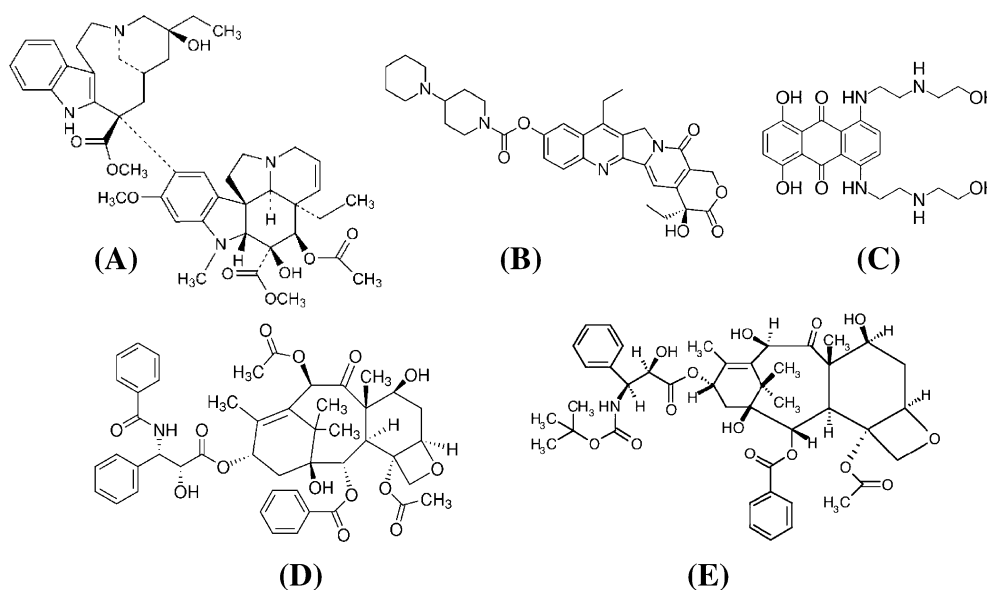
USA) at 25°C, as previously detailed (8). Zeta potential was determined in PBS solutions lacking NaCl, under a 3V/cm e-field, using phase analysis mode. The zeta potential was calculated from the electrophoretic mobility (EM) using the Smoluchowski model. (This was a reasonable approximation (22) given that the radius of the particles was predominantly between 50 and 1,000 nm, and the ionic strength during the EM measurement was calculated to be about 50 mM; that is, the Debye length (κ^{-1}) was around 1.4 nm, so that the product (κa) ranged between 35 and 700, i.e. $\kappa a \gg 1$).

RESULTS

Analysis of the Affinity and Stoichiometry of Drug Binding to β–CN

The interaction between each anticancer drug and β–CN was followed by absorbance spectra analysis. The drug-β–CN complex peak wavelength was compared to the peak wavelength of the mathematical summation of the absorbance spectra of pure β–CN and pure drug (each in PBS with same DMSO concentration). Absorbance spectra of 167 μM pure drug and of 1 mg/ml (0.042 mM) pure β–CN, and of 167 μM drug in 1 mg/ml β–CN, as well as the mathematical summation of the former two spectra were determined. Figure 3 presents absorbance spectra indicating the entrapment of paclitaxel in β–CN as detailed above; Fig. 3 shows that the spectrum of absorbance of entrapped paclitaxel in β–CN at a 4:1 molar ratio is shifted to a higher wavelength ("red-shifted") with respect to the mathematical summation of the pure β–CN and paclitaxel absorbance spectra. The spectral data around the peak absorbance was fit by a 5th degree polynomial, and the wavelength of maximum absorbance was determined. Similar curves were obtained for all studied drugs. The red shift in absorbance
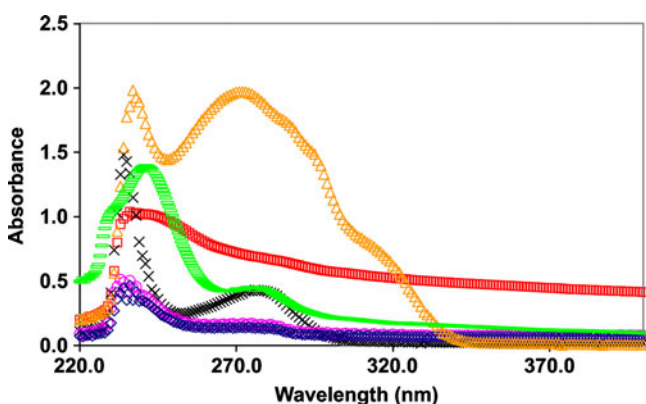
Fig. 2 Spectra of absorbance of 167 μM pure paclitaxel (□), docetaxel (○), vinblastine (△), irinotecan (◇), 42 μM mitoxantrone (8) (━) and 1 mg/ml (42 μM) pure β–CN (x).

peak of β–CN-drug complex was plotted vs. the calculated log P for all drugs and is presented in Fig. 4.

The molecular interactions occurring between β–CN and either paclitaxel or vinblastine were studied by measuring the Trp 143 fluorescence emission quenching by the drugs, as we have previously shown for the interaction of mitoxantrone with β–CN (8,9). The quenching of Trp fluorescence following the additions of docetaxel or irinotecan was insignificant (results not shown), probably because (unlike vinblastine, paclitaxel and mitoxantrone) docetaxel and irinotecan do not absorb at the Trp emission wavelength (332 nm) as shown in Fig. 2. Hence, it can be suggested that the quenching of Trp fluorescence possibly occurs via a mechanism of fluorescence resonance energy transfer (FRET). Figure 5 shows a decrease in Trp143 emission intensity upon a 287 nm excitation and 332 nm emission as a function of the drug:β–CN molar ratio ranging from 0.2:1 to 12:1 at 1 mg/ml β–CN. Approximately 80% of the initial overall Trp143 fluorescence intensity was quenched by vinblastine and mitoxantrone (8), and 35% was quenched by paclitaxel. The apparent association constant (K_a) and the number of drug molecules which were involved in this association process with β–CN micelles, per protein molecule for each drug, were calculated from the model fit (Eq. 1), and the results are presented in Fig. 6. It appears that the more hydrophobic the drug, the higher its stoichiometric association ratio, n (drug:β–CN molar ratio at maximal capacity), and the lower its Ka (association constant to a β–CN binding site, assuming a single affinity-class of sites).

Zeta Potential Analysis

Zeta potential measurements of pure drug solutions in PBS and in 1 mg/ml β–CN solutions vs. increasing drug concentrations (0–500 μM) and drug:protein molar ratios are presented in Fig. 7, for irinotecan, vinblastine, paclitaxel, docetaxel, and mitoxantrone (which we studied previously (8)). The figure reveals that in the concentration range studied here, all drugs in PBS showed zeta potential values above −40 mV. However, in the presence of 1 mg/ ml β–CN, the zeta potentials of practically all drug-β–CN systems in the studied concentrations were below −40 mV (except for mitoxantrone at high mitoxantrone:β–CN ratios).

The drugs can be classified into two groups, charged and uncharged (at pH 7.0). The drug-β–CN nanoparticles obtained with the uncharged drugs, including paclitaxel and docetaxel, showed close to constant zeta potential values of around −60 mV in all drug concentrations studied, similar to that of pure β–CN solution. In contrast, β–CN complexes of the charged drugs, mitoxantrone vinblastine and irinotecan showed nearly constant zeta
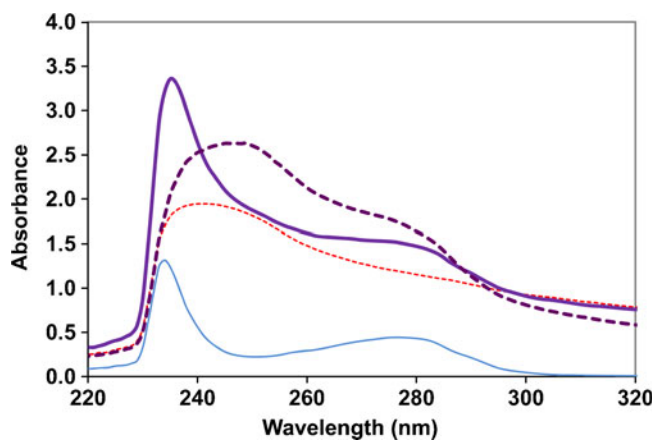
Fig. 3 Spectra of absorbance of 167 μM pure paclitaxel (*fine dashed red line*), 1 mg/ml pure β–CN (*fine solid blue line*), 167 μM paclitaxel in 42 μM β–CN complex (4:1 paclitaxel: β–CN molar ratio), (*thick dashed purple line*) *vs.* a mathematical summation plot of the former two spectra (*thick solid purple line*).

potential up to "critical" drug:β–CN molar ratios, above which the zeta potential of the complexes increased. These "critical ratios" were about 3:1, 3:1 and 4:1 for mitoxantrone, vinblastine, and irinotecan, respectively. Mitoxantrone-β–CN complexes showed the highest initial zeta potential values (about −40 mV), as well as the most significant rise above the critical ratio, hence reaching near zero values around 8:1 ratio. It should be noted that zeta potential values are averaging all particles in the system, including free protein, free drug and complexes. Based on the good affinity found between the drug(s) and the protein, it is reasonable to interpret the zeta potential results as mainly referring to nanocomplexes comprising both components (except only at very high or very low ratios). Moreover, in the case of positively charged drugs, the fact that plateaus were observed during drug addition (rather than a linear increase, expected for mixtures of non-interacting particles) over significant titration ranges is by itself an indication of complex formation, with the drug entrapped inside, not raising the surface charge (8).

It is noteworthy that pure solutions of un-encapsulated positively charged drugs in PBS, i.e. vinblastine, mitoxantrone, and irinotecan (Table I), showed unexpected negative zeta potential values. This may be explained by the presence of multivalent anions of the phosphate buffer, which presumably adsorb onto the positive drug aggregates and decrease their zeta potential to below zero (an overcharging effect). When pure irinotecan solutions at the same concentrations were measured in water (i.e. in the absence of phosphate buffer), the zeta potential was around 0 mV, compared to −25 mV in PBS (results not shown). Expectedly, the zeta potential in solutions of pure vinblastine, the most positively charged drug studied at pH 7 (+4.73), increased as a function of concentration.

Evaluation of Nanoparticle Size Distributions by DLS

The results obtained from the DLS analysis of the nanoparticle size distributions are presented in Figs. 8 (mean Gaussian diameter) and 9 (Nicomp™ volume-weighted particle size distributions). The mean Gaussian diameters of irinotecan-β–CN and of docetaxel-β–CN nanoparticles were rather constant up to a drug:β–CN molar ratio of 3:1 and increased above this ratio. The paclitaxel-β–CN nanoparticles and the vinblastine-β–CN nanoparticles had a lower mean Gaussian diameter at high drug:β–CN molar ratio than irinotecan-β–CN and docetaxel-β–CN complexes: 200 nm *vs.* 900 nm and 1,500 nm, respectively. Paclitaxel-β–CN and vinblastine-β–CN nanoparticles had approximately constant mean Gaussian diameters of around 100 nm and 150 nm, respectively, up to their maximal loading; above the maximal loading, particle sizes rose to approximately constant mean Gaussian diameters of 200 nm and 260 nm, respectively, and were hence consistent with our previous results obtained with mitoxantrone (8,9), which are drawn here too, although with MX there was a more pronounced rise above the maximal loading ratio. Nicomp™ volume-weighted particle size distributions of the drugs encapsulated in 1 mg/ml β–CN (Fig. 9) reveal that at low drug concentrations, the particle size distributions were either mono- or bi-modal for all drugs, and above 80% of the particles were smaller than 100 nm. At high drug concentrations bi- or tri-modal distributions were observed for all drugs, and larger particles were formed.

Colloidal Stability Evaluated by Visual Observation

Figure 10 shows photographs of 83.3 μM paclitaxel, 500 μM docetaxel and 500 μM irinotecan solutions in
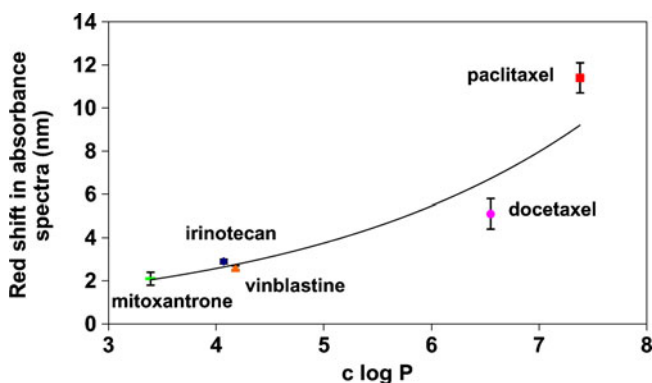
Fig. 4 Red shift in absorbance spectrum (nm) of β–CN-drug complex relative to the mathematical summation of its components *vs.* the calculated c log P of each drug. Drugs were in 1 mg/ml β–CN solutions. Paclitaxel, docetaxel, vinblastine, and irinotecan were at 4:1 drug: beta casein molar ratio and mitoxantrone was at 1:1 drug: beta casein molar ratio. (An exponential curve-fit is drawn as a guide to the eye.)
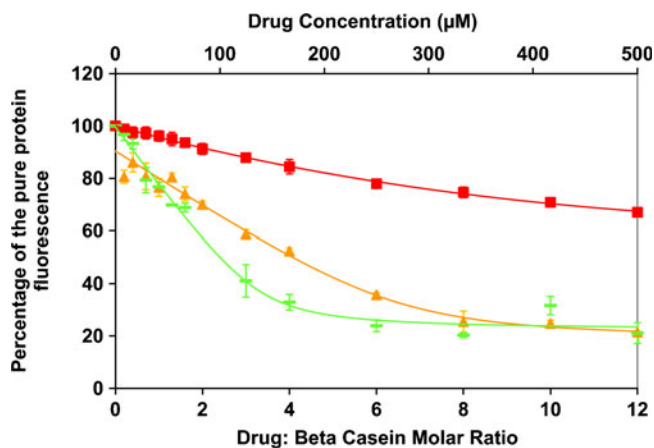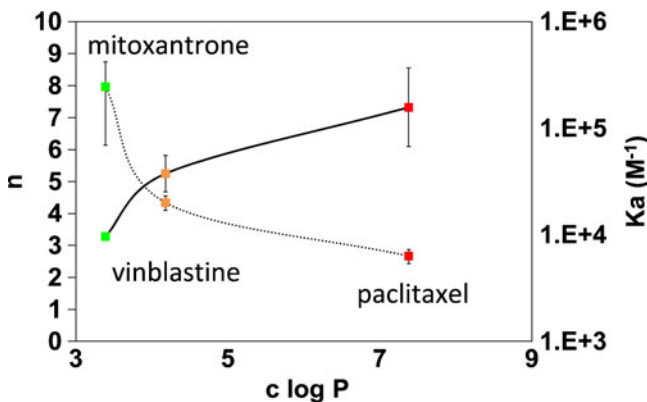
Fig. 5 Percentage of the initial Trp 143 emission as a function of drug concentration (*top axis*) and drug: β–CN molar ratio (*bottom axis*) of paclitaxel (■), vinblastine (▲), and mitoxantrone (9) (▬) in a 1 mg/ml β–CN solution. (Excitation: 287 nm and emission: 332 nm.) Line represents the model fit.

Fig. 7 Zeta potential of paclitaxel (■), docetaxel (●), vinblastine (▲), and irinotecan (◆) and mitoxantrone (▬) in 1 mg/mL β–CN complex *vs.* the drugs in PBS (*corresponding empty symbols*) as a function of drug concentration (*top axis*) and drug: β–CN molar ratio (*bottom axis*).
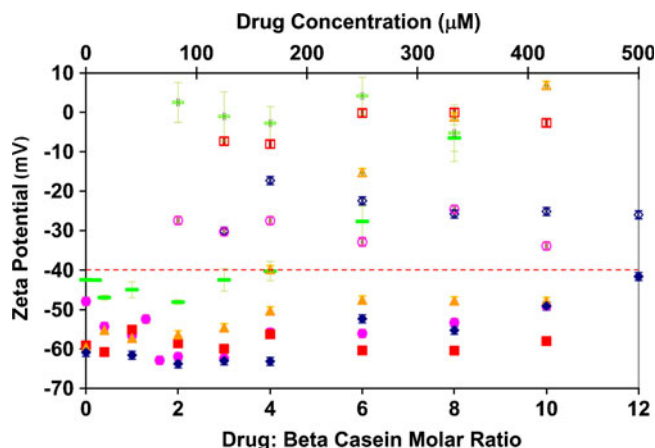
PBS compared to the respective drugs at the same concentrations entrapped in 1 mg/ml β–CN at 2:1, 12:1, and 12:1 drug: β–CN molar ratios, respectively. It is apparent from this figure that all pure drugs in PBS formed visible aggregates, while these drugs at the same concentrations entrapped in 1 mg/ml β–CN solution formed colloidally stable and much clearer solutions.

DISCUSSION

The primary aim of the current study was to identify the main physico-chemical properties of selected hydrophobic anticancer drugs, which affect the co-assembly process with β–CN. The structure formulae and the properties studied
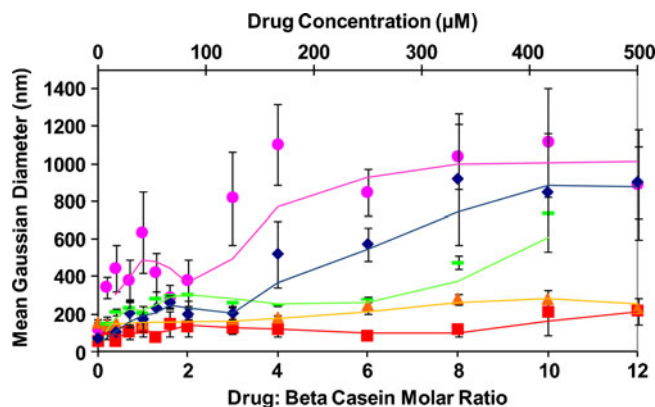
herein are summarized in Fig. 1 and Table I, respectively. We hypothesized that the main properties governing the co-assembly with the protein are hydrophobicity, as may be quantified by their calculated log P values, as well as their charge at pH 7, which may be calculated based upon the pKa values of all their ionizable groups. The order of increasing hydrophobicity of these drugs according to their c log P values is as follows: mitoxantrone < irinotecan < vinblastine < docetaxel < paclitaxel. The calculated log P values of mitoxantrone, vinblastine, paclitaxel and docetaxel are higher than those derived experimentally in the literature (see Table I for references), and there are sometimes significant differences between experimental data reported by different groups. Therefore, we chose to use calculated values, all obtained by the same software, to obtain a comparable database. The order of the calculated

Fig. 6 The apparent association constants K_a (dotted line) and the numbers of quencher (drug) molecules involved in the association with β–CN n (=drug: β–CN molar ratio at maximal capacity, solid line), obtained from the model fits to Trp143 fluorescence emission quenching by different drugs, as a function of the drugs' c log P.

Fig. 8 Mean Gaussian diameter of paclitaxel (■), docetaxel (●), vinblastine (▲), and irinotecan (◆) and mitoxantrone (8) (▬) in 1 mg/mL β–CN as a function of drug concentration (*top axis*) and drug: β–CN molar ratio (*bottom axis*). Moving average trendlines are drawn as a guide to the eye.

charge of the drugs at pH 7, based on the calculated pKa values of the various groups, in decreasing positive charge order is vinblastine > mitoxantrone > irinotecan > paclitaxel ≈ docetaxel ≈0.

Binding, Hydrophobicity and Charge

The first interesting observation we made (Fig. 4) was that the more hydrophobic the drug (as expressed by the higher c log P value), the higher the red shift of the drug-β–CN complex absorbance peak compared to the peak of the mathematical

summation of its components. When the local environment of the polypeptide chain becomes more hydrophobic, its absorbance is red-shifted (23). Hence, when a more hydrophobic drug is bound to the hydrophobic domain of β–CN, its absorbance is consequently shifted to longer wavelengths.

Considering the fluorescence-based binding results, our results are in accord with those of a recent study (24) using casein micelles to encapsulate curcumin, a natural spice with anticancer properties, where the authors reported a hydrophobic association, with a binding constant of $1.48*10^4 \, M^{-1}$. This value is in the same order of magnitude
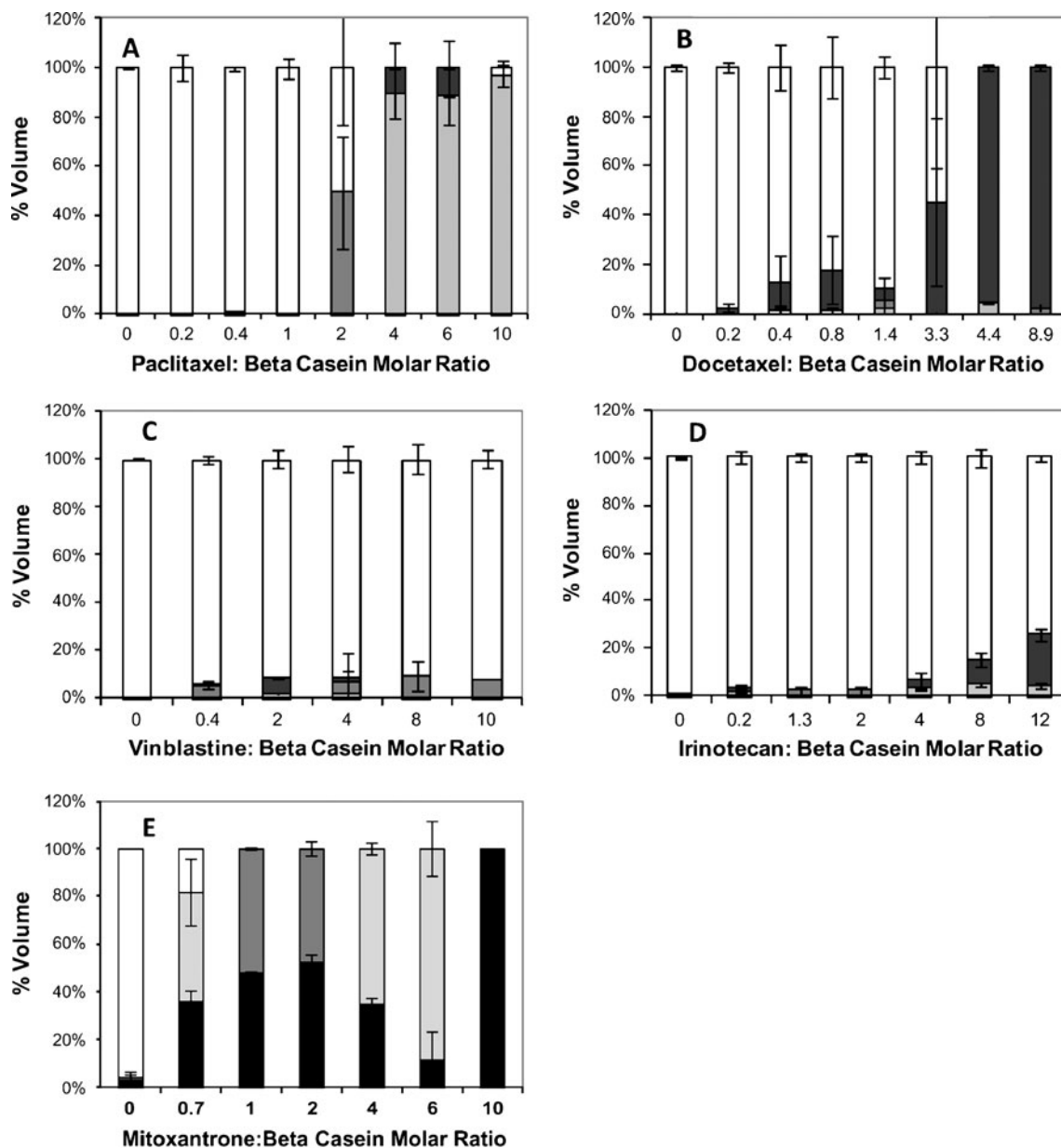
Fig. 9 Drug- β–CN particle size distribution. Volume percentage as a function of drug: β–CN molar ratio, in 1 mg/ml β–CN. (□) 0–100 nm, (▨) 100–200 nm, (▦) 200–300 nm, (■) 300 nm and up. (**A**) paclitaxel- β–CN nano particles, (**B**) docetaxel- β–CN nano particles, (**C**) vinblastine- β–CN nano particles, (**D**) irinotecan- β–CN nano particles and (**E**) mitoxantrone- β–CN nano particles (8).

as some of the cytotoxic drugs we have studied here (e.g. vinblastine, and paclitaxel, Fig. 6).

Another interesting finding is the more dramatic Trp 143 fluorescence quenching induced by the positively charged chemotherapeutic agents, including mitoxantrone and vinblastine, compared to that of the uncharged paclitaxel (Fig. 5, Table I). Apparently, beyond the Van derWaals and dispersion-forces interactions of all three drugs with the core of β–CN micellar nanoparticles, the positively charged drugs have a more "intimate" contact with the protein as they may also bind via electrostatic interactions to the negatively charged surface of the β–CN particles, whose charge is dominated by the serine-phosphate groups in the hydrophilic N-terminal domain of the protein. It is therefore reasonable to suggest that the electrostatic binding regions on β–CN are located close enough to contribute to Trp143 fluorescence quenching. Moreover, the increased fluorescence quenching may be partly due to the formation of larger particles formed by mitoxantrone and vinblastine, compared to those by paclitaxel, as seen in Fig. 8. Larger particles both block the light from reaching their core or escaping from it, and they scatter more light compared to smaller particles.

Figure 6 reveals that the more hydrophobic the drug, the higher the "n" value (drug: β–CN molar ratio at maximal capacity) and the lower its Ka value (association constant at an average β–CN binding site). This may be due to the binding of larger drug droplets of the more hydrophobic drugs per β–CN binding site. However, the association constant between one quencher molecule and the β–CN binding site near Trp143 is lower, as drug-drug association is also involved, which is likely to be weaker than protein-drug attraction.

Re-evaluation of our Previously Proposed Model

We have recently proposed a model (8) of clustering of drug-loaded micellar nanoparticle to explain mitoxantrone-β–CN co-assembly along with the fact that the surface charge, as deduced from zeta potential measurements, remains constant up to about the maximal loading, after which both the surface charge and the particle size increase (see mitoxantrone results in Figs. 7 and 8, respectively). The underlying premise was that hydrophobic associations are quicker than electrostatic interactions, because the former are less site specific, and they do not require a preceding dissociation process. Thus, upon addition of a drug that is pre-dissolved in an anhydrous water-miscible solvent (e.g. DMSO or ethanol), while stirring into the aqueous β–CN solution, we had assumed that as the solvent dissipates, the drug would first associate with the hydrophobic domains of the β–CN protein. At higher drug:protein ratios, as the hydrophobic domains of the protein have been saturated, electrostatic drug-protein association will likely lead to clustering of the initial micellar nanoparticles. In the current study, we tested this model for other drugs, some of which are both hydrophobic and positively charged, similarly to mitoxantrone, (e.g. vinblastine and irinotecan), whereas others are hydrophobic but uncharged (docetaxel and paclitaxel). Whilst most drugs followed these expected trends, a few behaved differently. The zeta potential graphs (Fig. 7) of the positively charged drugs—vinblastine and irinotecan—expectedly showed a low and constant plateau up to around their "core-saturation" (around 3:1 and 4:1 molar ratios respectively), followed by a rise, though this rise was not as steep as that of mitoxantrone. Particle size (Figs. 8 and 9) of irinotecan-loaded nanoparticles showed a considerable rise, like mitoxantrone, while the increase in particle size of vinblastine-loaded nanoparticles was much more moderate.

The zeta potential values of the uncharged hydrophobic drugs paclitaxel and docetaxel, in β–CN, were rather constant (around that of the pure protein: −50 to −60 mV) as their concentrations increased, in line with our prediction. However, the particle size distributions of
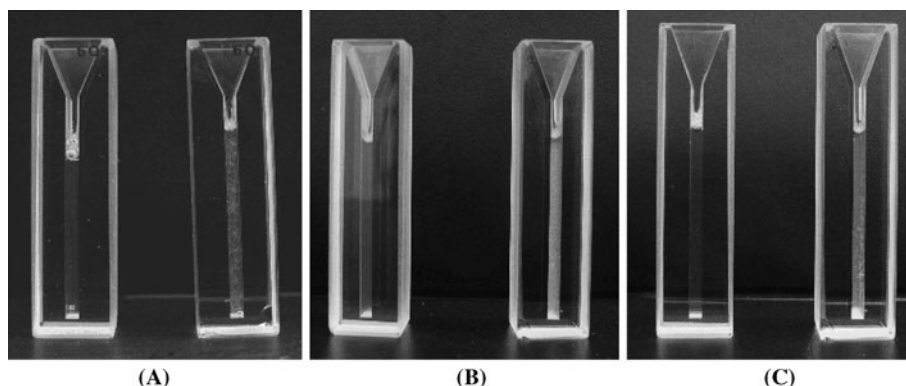
Fig. 10 Picture of 83.33 μM paclitaxel (**A**), 500 μM docetaxel (**B**), and 500 μM irinotecan (**C**) in 1 mg/ml (41.67 μM) β–CN solution (2:1, 12:1, 12:1 drug: β–CN molar ratio respectively) (*left*) *vs.* pure drug in PBS at the same concentration as in β–CN solution (*right*).

paclitaxel and docetaxel behaved quite differently. While paclitaxel expectedly showed initially small monomodal, particle sizes up to 2:1, then mainly bimodal, but still quite small particle sizes up to high (12:1) molar ratios, docetaxel, a rather closely related compound, unexpectedly showed bimodal distributions with substantially larger particles (~400 nm) already at rather low ratios (0.2–1.4), and an increase to around a micron above 3:1 ratio. Clearly, another unaccounted-for characteristic of the drugs also affected system behavior. Such an important structural feature, not readily quantifiable from the molecular structure, is the amphiphilicity of the drug molecule, which affects its packing parameter (25,26), self-assembly in pure aqueous solutions, and co-assembly with the protein. Comparing the structural formulae of paclitaxel and docetaxel, it is noticeable that the former has three benzene rings, and the latter only two. The arrangement of these three rings in paclitaxel appears to form a more dominant hydrophobic domain on the opposite side from the hydrophilic domain, making it more amphiphilic than docetaxel, in which polar and apolar groups are more evenly distributed in the structure.

A Complementary Model

We propose an additional model (Fig. 11) to provide a possible explanation for the difference between the behavior of paclitaxel and docetaxel. Upon dissipation of the stock solution and dilution of the water-miscible pre-solvent, the more hydrophobic the drug, the more likely it is to self-associate first, before interacting with the protein. Additionally, the more amphiphilic the drug is, the smaller its primary droplets, which form prior to protein entrapment (Fig. 11B). This would explain the much larger docetaxel nanoparticles, which formed already at low drug concentration. Further studies are underway to elucidate this peculiar behavior of docetaxel, including the use of imaging of the complexes by cryogenic transmission electron microscopy (cryoTEM), as well as measurement of surface and self assembly properties. Still, their entrapment by the protein (Fig. 11C) provides colloidal stability owing to the strong negative zeta potential and protein amphiphilicity. This is evident both from the clear-cut grouping of pure drug dispersions in PBS, having zeta potential values above −40 mV, considered the limit of colloidal stability (27), and the protein-stabilized systems, which were all below that threshold (except for mitoxantrone at high excess). The pure drugs in PBS were colloidally unstable and tended to aggregate and precipitate, while in the presence of only 1 mg/ml β–CN, much clearer stable solutions were obtained (see Fig. 10).
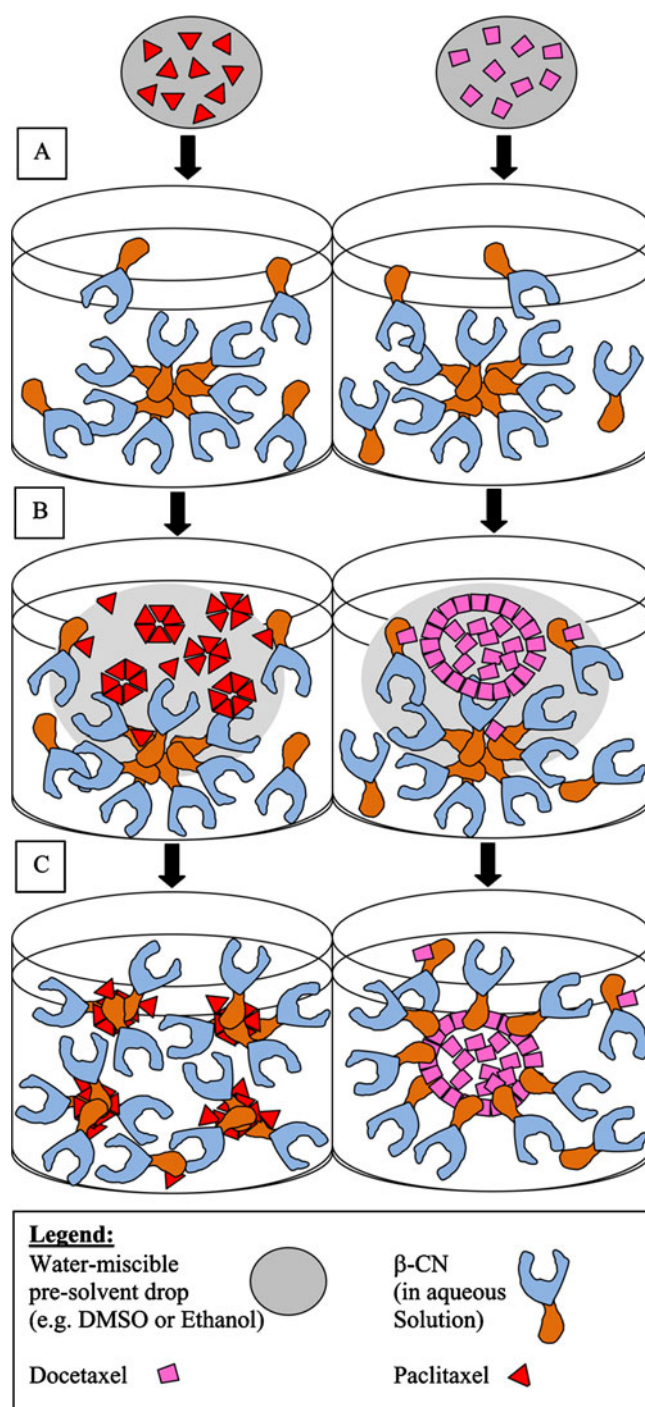
Fig. 11 A schematic diagram modeling the proposed sequence of events occurring during addition of the uncharged hydrophobic drugs, dissolved in a water-miscible solvent (DMSO or ethanol) into aqueous β–CN solution: **A**. The two drugs are well dissolved in the solvent. **B**. Upon addition to the aqueous solution, the solvent starts dissipating, and the drugs consequently self-assemble by the hydrophobic effect. Apparently, the geometry and better amphiphilicity of paclitaxel causes it to form smaller "primary micellar aggregates" compared to docetaxel. **C**. β–CN then "wraps" these primary aggregates, and stabilizes them, preventing their further aggregation. The smaller primary particles formed by paclitaxel result in smaller final nanocapsules.

CONCLUSIONS

Beta–CN displays a very good binding and entrapment capacity for this assortment of model hydrophobic anticancer drugs and thus may serve as a useful nanoscopic vehicle for the aqueous solubilization and stabilization in oral delivery preparations of these antitumor agents and possibly other hydrophobic therapeutic drugs aimed at treating malignant and non-malignant disorders. The fact that β–CN is a natural self-assembler, in addition to the notion that its open tertiary structure (due to the multiple proline residues present) has evolved to be easily digestible by gastric proteases, renders β–CN nanoparticles an excellent potential vehicle for targeting gastric diseases, including gastric cancer, which is a major cause of cancer death worldwide.

ACKNOWLEDGEMENTS

REFERENCES

1. Liu G, Franssen E, Fitch MI, Warner E. Patient preferences for oral *versus* intravenous palliative chemotherapy. J Clin Oncol. 1997;15:110–5.
2. Livney YD, Schwan AL, Dalgleish DG. A study of beta-casein tertiary structure by intramolecular crosslinking and mass spectrometry. J Dairy Sci. 2004;87:3638–47.
3. Swaisgood HE. Chemistry of the caseins. In: Fox PF, and McSweeney PLH, editors. Advanced dairy chemistry, volume 1, proteins, part A. New York: Kluwer Academic/Plenum Publishers; 2003. p. 139–201.
4. Mikheeva LM, Grinberg NV, Grinberg VY, Khokhlov AR, de Kruif CG. Thermodynamics of micellization of bovine β-casein studied by high-sensitivity differential scanning calorimetry. Langmuir. 2003;19:2913–21.
5. Dauphas S, Mouhous-Riou N, Metro B, Mackie AR, Wilde PJ, Anton M, et al. The supramolecular organisation of beta-casein: effect on interfacial properties. Food Hydrocolloids. 2005;19:387–93.
6. Portnaya I, Cogan U, Livney YD, Ramon O, Shimoni K, Rosenberg M, et al. Micellization of bovine beta casein studied by isothermal titration microcalorimetry and cryogenic transmission electron microscopy. J Agric Food Chem. 2006;54:5555–61.
7. Semo E, Kesselman E, Danino D, Livney YD. Casein micelle as a natural nano-capsular vehicle for nutraceuticals. Food Hydrocolloids. 2007;21:936–42.
8. Shapira A, Assaraf YG, Livney YD. Beta-casein nano-vehicles for oral delivery of chemotherapeutic drugs. Nanomed Nanotechnol Biol Med. 2010;6:119–26.
9. Shapira A, Markman G, Assaraf YG, Livney YD. β-casein based nanovehicles for oral delivery of chemotherapeutic drugs: drug-protein interactions and mitoxantrone loading capacity. Nanomed Nanotechnol Biol Med. In Press, doi:10.1016/j.nano.2010.01.003.
10. Forrest SA, Yada RY, Rousseau D. Interactions of vitamin D3 with bovine β-lactoglobulin A and β-casein. J Agric Food Chem. 2005;53:8003–9.
11. Lietaer E, Poiffait A, Adrian J. Interaction between casein and vitamin A. Lebens Wissen Technol. 1991;24:39–45.
12. Clark DC, Wilde PJ, Wilson DR, Wustneck R. The interaction of sucrose esters with β-lactoglobulin and b-casein from bovine milk. Food Hydrocolloids. 1992;6:173–86.
13. Horne DS. Casein structure, self-assembly and gelation. Curr Opin Colloid Interface Sci. 2002;7:456–61.
14. Zana R. Dynamics in micellar solutions of amphiphilic block copolymers. In: Hubbard AT, editor. Dynamics of surfactant self-assemblies. New York: CRC Press, Taylor & Francis Group; 2005. p. 161–231.
15. Etievant C, Barret JM, Kruczynski A, Perrin D, Hill BT. Vinflunine (20′, 20′-difluoro-3′, 4′-dihydrovinorelbine), a novel Vinca alkaloid, which participates in P-glycoprotein (Pgp)-mediated multidrug resistance *in vivo* and *in vitro*. Investig New Drugs. 1998;16:3–17.
16. Iyer SS, Gao S, Zhang ZP, Kellogg GE, Karnes HT. A molecular model to explain paclitaxel and docetaxel sensitivity changes through adduct formation with primary amines in electrospray ionization mass spectrometry. Rapid Commun Mass Spectrom. 2005;19:1221–6.
17. Pommier Y, Leo E, Zhang H, Marchand C. DNA Topoisomerases and their poisoning by anticancer and antibacterial drugs. Chem Biol. 17:421–33.
18. Vecchione L, Orditura M, Ciardiello F, De Vita F. Novel investigational drugs for gastric cancer. Expert Opin Investig Drugs. 2009;18:945–55.
19. I.A.I.-L.W.s. Advanced Chemistry Development. ACD/Labs Online (I-Lab) (ACD/Log P 8.02). http://ilab.acdlabs.com/ (accessed 2009).
20. Cogan U, Kopelman M, Mokady S, Shinitzky M. Binding affinities of retinol and related compounds to retinol binding proteins. Eur J Biochem. 1976;65:71–8.
21. Christiaens B, Symoens S, Vanderheyden S, Engelborghs Y, Joliot A, Prochiantz A, et al. Tryptophan fluorescence study of the interaction of penetratin peptides with model membranes. Eur J Biochem. 2002;269:2918–26.
22. Delgado AV, Gonzalez-Caballero E, Hunter RJ, Koopal LK, Lyklema J. Measurement and interpretation of electrokinetic phenomena—(IUPAC technical report). Pure Appl Chem. 2005;77:1753–805.
23. Hu Y-J, Liu Y, Wang J-B, Xiao X-H, Qu S-S. Study of the interaction between monoammonium glycyrrhizinate and bovine serum albumin. J Pharm Biomed Anal. 2004;36:915–9.
24. Sahu A, Kasoju N, Bora U. Fluorescence study of the curcumin-casein micelle complexation and its application as a drug nanocarrier to cancer cells. Biomacromolecules. 2008;9:2905–12.
25. Nagarajan R. Molecular packing parameter and surfactant self-assembly: the neglected role of the surfactant tail. Langmuir. 2002;18:31–8.
26. Kunz W, Testard F, Zemb T. Correspondence between curvature, packing parameter, and hydrophilic-lipophilic deviation scales around the phase-inversion temperature. Langmuir. 2009;25:112–5.
27. ASTM. Standard Test Methods for Zeta Potential of Colloids in Water and Waste Water, American Society for Testing and Materials (ASTM) Standard D 4187-82, *The Annual Book of ASTM Standards*, American Society for Testing and Materials, ASTM

International, 100 Barr Harbor Drive, PO Box C700, West Conshohocken, PA, 19428-2959 USA, 1985.

28. Gaertner L, Murray C, Morris C. Transepithelial transport of nicotine and vinblastine in isolated malpighian tubules of the tobacco hornworm (Manduca sexta) suggests a P-glycoprotein-like mechanism. J Exp Biol. 1998;201:2637–45.

29. Yang X-X, Hu Z-P, Xu A-L, Duan W, Zhu Y-Z, Huang M, *et al.* A mechanistic study on reduced toxicity of irinotecan by coadministered thalidomide, a tumor necrosis factor-{alpha} inhibitor. J Pharmacol Exp Ther. 2006;319:82–104.

30. Dicko A, Tardi P, Xie X, Mayer L. Role of copper gluconate/triethanolamine in irinotecan encapsulation inside the liposomes. Int J Pharm. 2007;337:219–28.

31. Saito H, Hirano H, Nakagawa H, Fukami T, Oosumi K, Murakami K, *et al.* A new strategy of high-speed screening and quantitative structure-activity relationship analysis to evaluate human ATP-binding cassette transporter ABCG2-drug interactions. J Pharmacol Exp Ther. 2006;317:1114–24.

32. Troy DB. Remington: the science and practice of pharmacy. Philadelphia: Lippincott Williams & Wilkins; 2005.

33. Sunil SI, Songmei G, Zong-Ping Z, Glen EK, Karnes HT. A molecular model to explain paclitaxel and docetaxel sensitivity changes through adduct formation with primary amines in electrospray ionization mass spectrometry. Rapid Commun Mass Spectrom. 2005;19:1221–6.